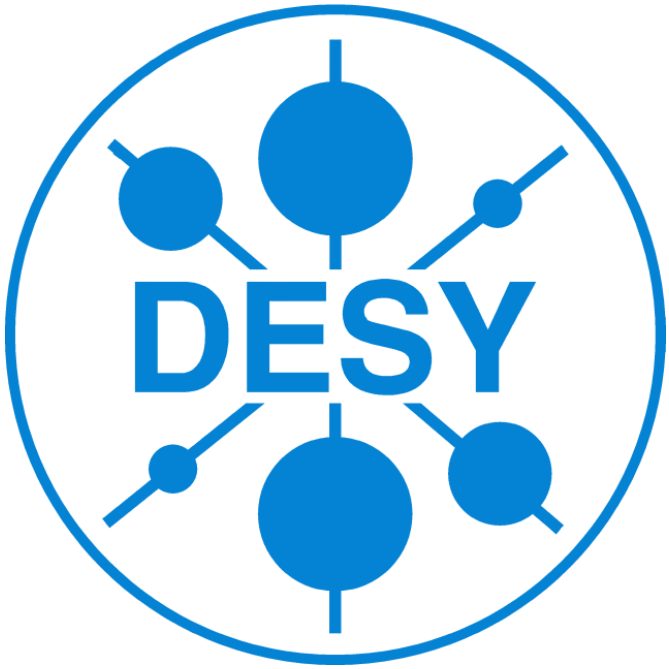

MONTE CARLO STUDY OF THE SECONDARY INTERACTIONS EFFECT IN OLYMPUS EXPERIMENT

05.09.2013

Voronezh state university, Russia
Evseev, Nickolai

Supervisor:

Naryshkine, Iouri

Contents

1. Introduction.

Recent determinations of the proton electric to magnetic form factor ratio from polarization transfer measurements indicate an unexpected and dramatic discrepancy with the form factor ratio obtained using the Rosenbluth separation technique in unpolarized cross section measurements. This discrepancy has been explained as the effects of multiple photon exchange beyond the usual one-photon exchange approximation in the calculation of the elastic electron-proton scattering cross section. Since most of our understanding on the structure of the proton and atomic nuclei is based upon lepton scattering analyzed in terms of the single photon approximation; it is essential to definitively verify the contribution of multiple photon exchange.

In June 2007, OLYMPUS collaboration submitted to DESY a letter of intent to carry out an experiment to definitively determine the contribution of multiple photon exchange in elastic lepton-nucleon scattering. The most direct evidence for multiple photon exchange would be a deviation from unity in the ratio of positron-proton to electron-proton elastic scattering cross sections. The experiment would utilize intense beams of electrons and positrons in the DORIS ring incident on an internal hydrogen gas target at an incident energy of 2.01 GeV and precisely measure elastic scattering at polar angles between 20 and 80 with high statistical and systematic precision. For this experiment we proposed to use the existing Bates Large Acceptance Spectrometer Toroid (BLAST) from MIT and an unpolarized internal gas target similar to one used by the HERMES experiment at HERA.

The OLYMPUS (pOsitron-proton and eLectron-proton elastic scattering to test the hYpothesis ofMulti-Photon exchange Using doriS) collaboration comprises over fifty physicists from fifteen institutions in Germany, Italy, Russia, the United Kingdom, and the United States.

The experiment takes advantage of unique features of the BLAST detector combined with an internal hydrogen gas target and the DORIS storage ring operated with both electrons and positrons. The systematic uncertainties are controllable at the percent level, and with the superior luminosity that can be provided at DORIS, this experiment will not be limited in statistical precision.

2. The OLYMPUS spectrometer.

The OLYMPUS experiment will take advantage of the existing BLAST detector which was successfully operated at the MIT-Bates Linear Accelerator Center. The BLAST detector as it was configured at MIT-Bates is shown in Figure 1. It was situated on the South Hall

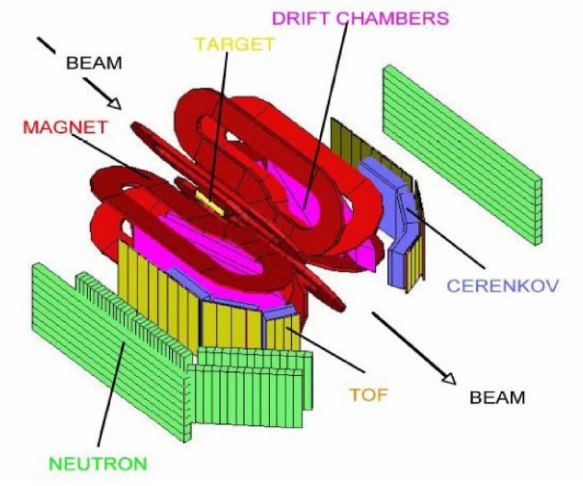

Figure 1: Schematic of the BLAST detector showing the main detector elements.

storage ring just downstream of the injection point. The detector was based upon an eight sector, toroidal, magnetic field. The two horizontal sectors were instrumented with detector components while the two vertical sectors were used by the internal targets and the vacuum system for the beamline.

The detector configuration we propose for OLYMPUS will use the BLAST toroidal magnet and instrument the horizontal sectors with the BLAST wire chambers and time of flight scintillators. As such the detector will be left/right symmetric. The drift chambers will provide charge particle tracking to determine the charge, momentum, scattering angles, and vertex for the charged particles produced. The time of flight scintillators will determine the relative timing of the reaction products and provide the trigger timing for the detector system.

The toroidal magnet shown in Fig. 2. was designed and assembled at MIT-Bates. A toroidal configuration was chosen to ensure a small field along the beamline to minimize effects on the beam transport and also to have small gradients in the region of the target cell. The magnetic field in the region of the drift chambers was used to momentum analyze the charged particles produced during the experiment. It also minimized the number of low energy charged particles reaching the detectors.

The toroid consists of eight copper coils placed symmetrically about the beamline. Each coil consists of 26 turns of hollow, 1.5 inch square copper tube organized into two layers of 13 turns. The copper tubes are wrapped with a fiberglass tape and then potted with epoxy resin. The coils are cooled by owing water through the hollow conductors. During the BLAST experiment the normal operating current was 6730 A resulting in a maximum field around 3.8 kG.

Figure 2: The eight coil BLAST toroid without its detectors.

The drift chambers shown in Figure 3. measured the momenta, charge, scattering angles, and vertices for the particles produced in the reactions studied with BLAST. This was done by tracking the charged particles in three dimensions through the toroidal magnetic field and reconstructing the trajectories. Measuring the curvature of the tracks yielded the particles momenta, and the directions of curvature determined their charge. Tracing the particles trajectories back to the target region allowed the scattering angles, polar and azimuthal, to be determined and the position of closest approach to the beam axis was taken as the vertex position for the event.

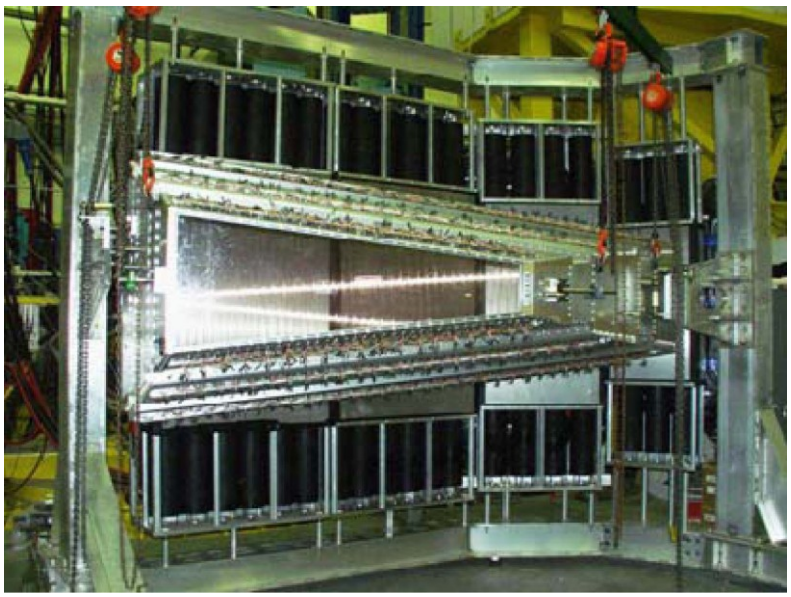

Figure 3: Photo of the BLAST drift chambers.

To maximize the active area, the drift chambers were designed to fit between the coils of the toroidal magnet such that the top and bottom plates of the drift chamber frame were in the shadow of the coils as viewed from the target. The drift chambers had a large acceptance and nominally subtended the polar angular range 20^0-80^0 and $\pm 15^0$ in azimuth with respect to the horizontal and were positioned and orientated such that 73.54^0 with respect to the beam from the target center was perpendicular to the face of the chambers. Because of these choices the chambers were trapezoidal in shape (see Figure 4.).

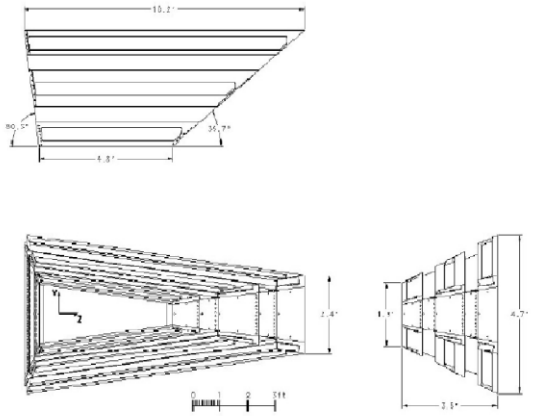

Figure 4: Top, bottom, and side views of the assembled drift chamber for a sector giving overall dimensions.

Each sector in BLAST contained three drift chambers (inner, middle, and outer) joined together by two interconnecting sections to form a single gas volume (see Figure 5.). This was done so that only a single entrance and exit window was required for the combined drift chambers thus minimizing energy loss and multiple scattering.

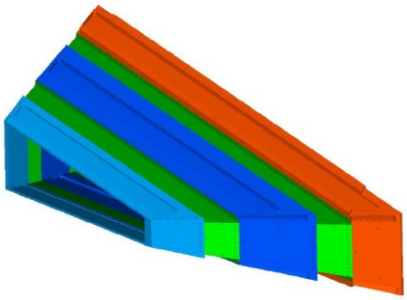

Figure 5: Isometric view of all three drift chambers assembled into a single gas volume.

Even with 18 planes of sense wires the track reconstruction was not straight forward. This was because the 6 sense wire planes in each of the three chambers in a sector were relatively close together and thus tended to yield a single point in space. Thus the track reconstruction had three space points with which to fit the momenta, scattering angles, charge, and vertex. And while this was possible there was no redundancy with which to measure of the accuracy of the reconstruction or to use the data to improve the track fitting parameters. Furthermore, if there was any additional hits in a chamber due to other tracks or noise these extra points could yield tracks that were not easily distinguished from the true tracks. Because of this we would like to add a triple GEM detector approximately 40 cm from the target in both sectors.

This detector would be 90 cm long and trapezoidal in shape varying from 18 to 36 cm in height. The frames of these triple GEM detectors would be in front of the toroid coils so would not reduce the active area. A conservative 2D readout design with 1 mm line pitch should give position resolutions on the order of 150 microns comparable to that of the wire chambers and require less than 1280 channels of readout.

The choice of GEM technology is based on the fact that GEM's are:
- thin - < 0.7% radiation length
- fast - can handle rates up to 500 kHz/cm2
- 2D - readout can provide both X and Y information
- compact - approximately 10 mm thick
- accurate - resolutions better than 50 microns are possible
- radiation tolerant
- insensitive to magnetic fields

In each sector of BLAST 16 vertical scintillator bars formed the time of flight (TOF) detector. The TOF detector was designed and produced at the University of New Hampshire to provide a fast, stable timing signal correlated with the time of each event at the target independent of which scintillator bar was struck. This signal was used to trigger the readout and data acquisition system for all other components and particularly provided the COMMON STOP signal for the drift chambers. This permitted relative timings among all components to be measured. The TOF detector also provided a measure of energy deposition to aid particle identification. Approximate position information was also possible from the timing difference between the top and bottom photomultiplier tubes.

In BLAST the TOF detector curved behind (see Figure 6) the wire chambers and Cerenkov detectors in each sector roughly matching the angular coverage of the tracking detector in both polar ($\sim 20^0 < \theta < \sim 80^0$) and azimuthal ($\pm \sim 15^0$) projections. The forward four bars at $\theta < 40^0$ were 119.4 cm high, 15.2 cm wide, and 2.54 cm thick. The remaining 12 bars at $\theta > 40^0$ were 180.0 cm high, 26.2 cm wide, and 2.54 cm thick. Bicron BC-408 plastic scintillator was chosen for its fast response time (0.9 ns rise time) and long attenuation length (210 cm). Each TOF

scintillator bar was read out at both ends via Lucite light guides coupled to 3 inch diameter, Electron Tubes1 model 9822B02 photomultiplier tubes, PMTs, equipped with Electron Tubes EBA-01 bases. The light guides were bent to point away from the interaction region so the PMT's would be roughly perpendicular to the toroidal magnetic field. Mu-metal shielding was used around all PMT's. The bases have actively stabilized voltage dividers so that the timing is independent of the gain.

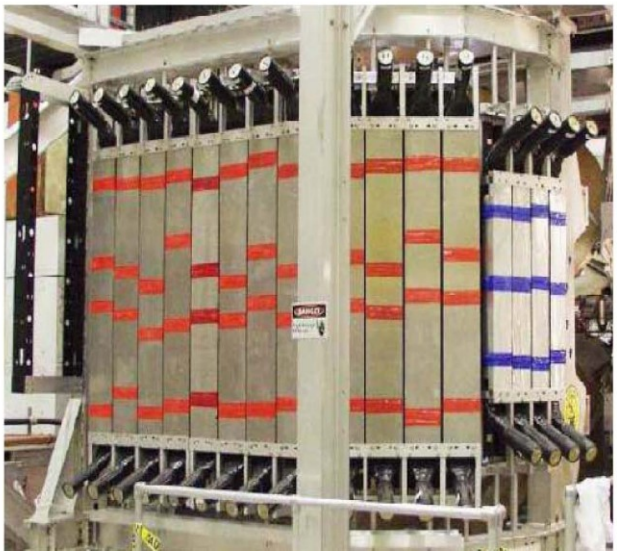

Figure 6: TOF detector mounted in sub-detector support during assembly.

3. Physics motivation

In the course of the more than 50 year long history of elastic electron-proton scattering since Hofstadter [3] the separation of the proton's electric and magnetic form factors, G^p_E (Q^2) and G^p_M (Q^2), has been of particular interest. These two functions of Q^2 describe the distribution of charge and magnetism of the proton and it is expected that precise ab initio calculations in terms of quarks and gluons will become available in the foreseeable future using lattice QCD techniques [4]. Until the 1990's the experimental method to separate $G_E(Q^2)$ and $G_M(Q^2)$ was based on the procedure by Rosenbluth [5] measuring the unpolarized elastic cross section at fixed four-momentum transfer, Q^2, but with different electron scattering angles and incident beam energies. It was found that the Q^2 dependence of both G_E and G_M, to a good approximation, followed the form of the Fourier transform of an exponentially decaying distribution, namely the dipole form factor $(1 + Q^2/0.71)^{-2}$, implying a ratio of $\mu G_E/G_M \approx 1$.
Due to the nature of the Rosenbluth formula

$$\frac{d\sigma/d\Omega}{(d\sigma/d\Omega)_{Mott}} = \frac{G_E^2(Q^2) + \tau G_M^2(Q^2)}{1+\tau} + 2\tau G_M^2(Q^2)\tan^2\frac{\theta}{2} = \frac{\epsilon\, G_E^2(Q^2) + \tau G_M^2(Q^2)}{\epsilon\,(1+\tau)}, \tag{3.1}$$

where $r = Q2/(4M^2_p)$, the transverse virtual photon polarization $\varepsilon = [1+2(1+ r)\tan^2(\theta/2)]^{-1}$, and $(d\sigma/d\Omega)Mott = \alpha^2/(4E^2)(\cos^2(\theta/2)/\sin^4(\theta/2)(E'/E)$; the weight of G_E in the cross section becomes less at higher Q^2 making the Rosenbluth separation of $G_E(Q^2)$ and $G_M(Q^2)$ at high momentum transfer rather difficult. While some experiments reported a scaling of the form factors; others occasionally observed significant deviations of the ratio $\mu G_E/G_M$ from unity. The world data for elastic e-p scattering has recently been compiled by [21]. The most recent Rosenbluth-type measurements have again confirmed the scaling behavior of the proton form factor ratio [7, 8], and additional unpolarized precision measurements are underway [22].

The generally accepted explanation for the discrepancy between the recoil polarization and Rosenbluth determinations of the elastic proton form factor ratio is the exchange of multiple (>1) photons during the electron-proton elastic scattering process [25, 35]. This implies that

certain lepton-nucleon scattering observables will differ significantly from their one-photon exchange (or first-order Born approximation) expectation value.

Multiple-photon exchange processes will exhibit a characteristic dependence of the elastic lepton-proton scattering cross section on the value of the virtual photon polarization, ε. As ε decreases, the effects of multiple-photon exchange on the elastic cross section tend to increase in magnitude.

The discrepancy between the recoil polarization and Rosenbluth determinations of the elastic proton form factor ratio grows with increasing Q^2. At high Q^2, the cross section is dominated by magnetic (i.e. transverse) scattering. This explains why the effect on the extraction of G_E from Rosenbluth separations can be sizable, while the effect on the cross section at all values of Q^2 is rather modest. At the same time, the form factor ratio from polarization experiments is less affected.

The effect of multiple-photon exchange on the electromagnetic elastic form factors involves the real part of the multiple-photon exchange amplitude. The observable most sensitive to this amplitude is the ratio of the elastic cross section for electron-proton to positron-proton scattering. In the presence of multiple-photon exchange, the cross section for unpolarized lepton-proton scattering contains an interference term between the one- and two-photon amplitudes. This interference is odd under time reversal, and hence has the opposite sign for elastic positron-proton and electron-proton scattering. Therefore, a non-zero two-photon amplitude would result in different cross sections for unpolarized electron-proton and positron-proton scattering.

The elastic form factors of the proton are defined in the context of the Born cross section, i.e. the single photon exchange term in the perturbative QED expansion. Corrections for radiative processes involving the incoming and outgoing charged particles must be applied to extract the Born cross section. These corrections are well understood and are calculable in QED.

The use of the intense, multi-GeV stored electron and positron beams at the storage ring DORIS at DESY, Hamburg, Germany in combination with the BLAST detector can produce the most definitive data to determine the effect of multiple photon exchange in elastic lepton-proton scattering and verify the recent theoretical predictions.

4. Control of Systematics

The primary observable of this experiment is the ratio of the electron-proton and positron-proton elastic cross sections. The redundant control measurements of the luminosity will allow the e^+p/e^-p cross section ratio to be determined with high precision.

As shown below, the individual proton and lepton detection efficiencies and the systematic errors associated with them will cancel to first order. However, acceptance effects need to be taken into account. In the OLYMPUS proposal [2], the effects on the cross section ratio due to slightly different acceptances for coincident detection of leptons and protons in the four beam species/magnet polarity combinations had been neglected. Below is laid out a scheme, how such acceptance effects can be accounted for explicitly.

The differential number of counts dN between times t and t + dt and in the detector volume element $d^n x$, using generalized detector coordinates x_k, is a function of efficiencies for proton and lepton detection, luminosity, differential cross section and acceptance and is given by

$$dN = \kappa^p(t)\kappa^l(t)\dot{L}(t)dt\ \frac{d\sigma}{d\Omega}(\theta_e)a(x_k)d^n x, \tag{4.1}$$

where k^p and k^l denote the proton and lepton detection efficiencies, which could generally vary with time, and L(t) is the instantaneous luminosity. The elastic differential cross section is denoted by $d\sigma/d\Omega$ and is only a function of one variable, e.g. the lepton scattering angle. The acceptance function a(xk) depends on all detector-related coordinates x_k, which can be lepton

and proton angles and momenta, or reconstructed vertices, etc., i.e. all degrees of freedom of a coincident lepton-proton event. For any given event, $a(x_k)$ describes whether or not it would be accepted by the detector, i.e. the acceptance function's value is either 0 or 1. It is the task of a Montecarlo simulation to determine the bin-averaged acceptance or phasespace integral.

To obtain the number of counts, Equation (1.2) needs to be integrated over the time $\Delta T = \int dt$ during which the data acquisition is alive, and over the detector volume $\Delta V = \int d^n x$. The elastic cross section $d\sigma/d\Omega$ is differential only in terms of the solid angle of the lepton. For integration over the detector volume, the acceptance function $a(x_k)$ describes the phasespace covered by the detection volume. As such the acceptance function also accounts for any kinematic correlations that are typical for elastic scattering events. Not the acceptance function itself, but only its integral over the detection volume (phasespace integral) is of interest for the analysis. The integration is carried out numerically by means of a Montecarlo simulation. Note that in addition to acceptance, the detection efficiencies are in the following accounted for explicitly.

Subsequently, the bin-averaged differential cross section equates to

$$\left\langle \frac{d\sigma}{d\Omega} \right\rangle = \frac{N}{\int_{\Delta T} \kappa^p(t)\kappa^l(t)\dot{L}(t)dt \int_{\Delta V} a(x_k)d^n x} . \tag{4.2}$$

In the denominator of Eq. (1.3) the bin-averaged differential cross section involves the integral of the acceptance function over the detector volume, which is commonly known as the phasespace integral

$$A = \Delta\Omega = \int_{\Delta V} a(x_k)d^n x. \tag{4.3}$$

For elastic scattering, the acceptance is identical with the solid angle $\Delta\Omega$ accepted in the considered bin.

If the period ΔT is short compared to the time scale within which the efficiencies vary, they can be considered constant in the integral of Eq. (1.3), and the time integral in the denominator results in the product of the time-averaged detection efficiencies $k^p * k^l$ and the integrated luminosity

$$L = \int_{\Delta T} \dot{L}(t)dt \tag{4.4}$$

over the measured period ΔT.

In order to reduce the systematic errors of the cross section ratio due to uncertainties in relative luminosity, acceptance and efficiency with individual electron and positron beams, we require that the beam in DORIS be alternated between electrons and positrons, and that the LYMPUS magnet polarity be reversed with the same frequency.

For a given bin, the number of events is hence given by

$$N_{ij} = L_{ij}\sigma_i\kappa^p_{ij}\kappa^l_{ij}A_{ij} , \tag{4.5}$$

where $i = e^+(e^-)$ for positrons (electrons) and j = +(-) for positive (negative) OLYMPUS magnetic field polarity. The integrated luminosity L is defined in Eq. (1.5), the bin-averaged lepton-nucleon elastic cross section is abbreviated as $\sigma = d\sigma/d\Omega$, the average efficiencies during the measurement period ΔT are k^p for detecting the recoil protons and k^l for the scattered leptons. The acceptance or phasespace integral is given by A as defined in Eq. (1.4).

With a given polarity of the OLYMPUS magnetic field, the efficiency for detecting the recoil protons in the same kinematics will be identical for both electron and positron scattering, namely: $k^p_{e+-} = k^p_{e-+}$ and $k^p_{e+-} = k^p_{e--}$. Hence, for a given field polarity, j, the proton efficiencies k^p_{ij} cancel in the ratio

$$\frac{N_{e+j}/L_{e+j}}{N_{e-j}/L_{e-j}} = \frac{\sigma_{e+}}{\sigma_{e-}} \cdot \frac{\kappa^l_{e+j}}{\kappa^l_{e-j}} \cdot \frac{A_{e+j}}{A_{e-j}} \,. \tag{4.6}$$

However, the efficiencies for detecting the scattered electron or positron may differ for a given OLYMPUS magnet polarity but will be the same for opposite polarities, namely: $k^p_{e+-} = k^p_{e-+}$ and $k^p_{e+-} = k^p_{e--}$. By taking the product of the above ratio for opposite magnetic field polarities yields

$$\frac{\sigma_{e+}}{\sigma_{e-}} = \left[\frac{N_{e++}\, N_{e+-}}{N_{e-+}\, N_{e--}} \Big/ \left(\frac{L_{e++}\, L_{e+-}}{L_{e-+}\, L_{e--}} \cdot \frac{A_{e++}\, A_{e+-}}{A_{e-+}\, A_{e--}} \right) \right]^{\frac{1}{2}} , \tag{4.7}$$

which measures the cross section ratio directly, where all lepton and proton efficiencies cancel out if they do not change during the length of the cycle of four combined states and if the reversal of the magnet polarity exactly reproduces the field amplitude. Equation (1.8) also contains the super ratio of the four phasespace integrals Aij , which has to be determined with Montecarlo simulations. In the central parts of the acceptance it is expected that the phasespace super ratio is close to unity. As Eq. (1.8) indicates, the relative luminosities in the form of ratios need to be known precisely for an accurate determination of the cross section ratio σ_{e+}/σ_{e-} . Only the combination of count rate super ratios, luminosity super ratios, and super ratio of phasespace integrals yields the final result. In the analysis of OLYMPUS each of the three super ratios in Eq. (1.8) will be determined individually, thereby "blinding" the result for the final cross section ratio until finally put together.

A similar consideration as in Eq. (1.6) also holds for the measurement and combination of the four luminosities, Lij , where the respective efficiencies cancel. In order to measure the relative luminosity, we propose to use elastic scattering at forward angle corresponding to small Q^2 and large ε where the effects of two-photon exchange are negligible. Subsequently, the cross section ratio σ_{e+}/σ_{e-} becomes unity, and hence the forward-angle coincident elastic rates N^{fwd}_{ij} are directly proportional to the luminosities in each of the four states {ij}

$$\frac{N^{fwd}_{e++}}{N^{fwd}_{e-+}} \cdot \frac{N^{fwd}_{e+-}}{N^{fwd}_{e--}} = \frac{L_{e++}\, L_{e+-}}{L_{e-+}\, L_{e--}} \cdot \frac{A^{fwd}_{e++}\, A^{fwd}_{e+-}}{A^{fwd}_{e-+}\, A^{fwd}_{e--}} \,, \tag{4.8}$$

which involves another super ratio of acceptances or phasespace integrals A^{fwd}_{ij} to be determined with Montecarlo simulations, now for the combination of the forward lepton detector in coincidence with proton in the OLYMPUS main detector. However, any dependence on the detection efficiencies for the forward lepton and recoil proton cancels out again. The final expression for the measured differential cross section ratio becomes

$$\frac{\sigma_{e+}}{\sigma_{e-}} = \left[\left(\frac{N_{e++}\, N_{e+-}}{N_{e-+}\, N_{e--}} \Big/ \frac{A_{e++}\, A_{e+-}}{A_{e-+}\, A_{e--}} \right) \Big/ \left(\frac{N^{fwd}_{e++}\, N^{fwd}_{e+-}}{N^{fwd}_{e-+}\, N^{fwd}_{e--}} \Big/ \frac{A^{fwd}_{e++}\, A^{fwd}_{e+-}}{A^{fwd}_{e-+}\, A^{fwd}_{e--}} \right) \right]^{\frac{1}{2}} . \tag{4.9}$$

The ratio of relative luminosities in Eq. (1.9) can be measured at sub-percent statistical errors in less than one hour. Thus, frequent and random filling with both e^+ and e^- beams and

reversal of the OLYMPUS field direction will minimize systematic uncertainties in the ratio from acceptance and efficiency differences as statistics are accumulated. The period for alternating beams and magnet polarities has to be short compared to the time over which effects due to detector performance, such as detection efficiencies, are likely to change. Within that time frame, target density and beam current fluctuations, however, are appropriately accounted for and will have no systematic effect. Some period on the order of one day would likely be sufficient. The systematic error of each super ratio measurement according to Eq. (1.10) can thus be reduced by the square root of the number of cycles through the four states {ij}.

Note the above derivation applies to the lepton detected in one sector of the OLYMPUS detector and the proton detected in the opposite sector. During the experiment, data will be collected simultaneously for leptons and protons detected in both sectors yielding another level of redundancy and cancellation of systematic effects.

The above scheme makes use of measurements of the proton and lepton tracks in coincidence. Further information and additional checks of systematics will be obtained from proton or lepton single-arm events for which the high and low ε limits of the OLYMPUS acceptance are extended. Provided that backgrounds in single-arm elastic events can be kept at a minimum, proton single-arm ratios for electron and positron beams with the same polarity of OLYMPUS, as well as lepton single-arm ratios with reversed field polarity also probe the e^+/e^- cross section ratio independently.

5. Monte Carlo

Monte Carlo methods (or Monte Carlo experiments) are a broad class of computational algorithms that rely on repeated random sampling to obtain numerical results; i.e., by running simulations many times over in order to calculate those same probabilities heuristically just like actually playing and recording your results in a real casino situation: hence the name. They are often used in physical and mathematical problems and are most suited to be applied when it is impossible to obtain a closed-form expression or infeasible to apply a deterministic algorithm. Monte Carlo methods are mainly used in three distinct problems: optimization, numerical integration and generation of samples from a probability distribution.

Monte Carlo methods are especially useful for simulating systems with many coupled degrees of freedom, such as fluids, disordered materials, strongly coupled solids, and cellular structures (see cellular Potts model). They are used to model phenomena with significant uncertainty in inputs, such as the calculation of risk in business. They are widely used in mathematics, for example to evaluate multidimensional definite integrals with complicated boundary conditions. When Monte Carlo simulations have been applied in space exploration and oil exploration, their predictions of failures, cost overruns and schedule overruns are routinely better than human intuition or alternative "soft" methods.

The modern version of the Monte Carlo method was invented in the late 1940s by Stanislaw Ulam, while he was working on nuclear weapon projects at the Los Alamos National Laboratory. It was named, by Nicholas Metropolis, after the Monte Carlo Casino, where Ulam's uncle often gambled. Immediately after Ulam's breakthrough, John von Neumann understood its importance and programmed the ENIAC computer to carry out Monte Carlo calculations.

Monte Carlo methods are very important in computational physics, physical chemistry, and related applied fields, and have diverse applications from complicated quantum chromodynamics calculations to designing heat shields and aerodynamic forms. In statistical physics Monte Carlo molecular modeling is an alternative to computational molecular dynamics, and Monte Carlo methods are used to compute statistical field theories of simple particle and polymer systems. Quantum Monte Carlo methods solve the many-body problem for quantum systems. In experimental particle physics, Monte Carlo methods are used for designing detectors,

understanding their behavior and comparing experimental data to theory. In astrophysics, they are used in such diverse manners as to model both the evolution of galaxies and the transmission of microwave radiation through a rough planetary surface. Monte Carlo methods are also used in the ensemble models that form the basis of modern weather forecasting.

In High Energy Physics the Monte Carlo simulations are usually used for acceptance function calculation and for systematic studies. For this purpose the OLYMPUS Monte Carlo program was developed in OLYMPUS collaboration. This program is based on elastic events generator, GEANT 4 toolkit to simulate particle propagation through the detector and calculate the response of detector's component on particle (digitization). The geometry and materials are describes the high precision of this program. Measured magnetic field of the spectrometer is all so used in the simulation. All secondary interactions for scattered electrons (positron) protons are included also. There two photon exchange in event generator, so the deviation of N_{e+}/N_{e-} ratio from the unity cod be caused only by the secondary interactions (as the numbers of generated samples for positron and electron beams are the same).

Because the elastic scattering of electrons and positrons interact differently with matter as it passes through the detector (the effect of annihilation of positrons which is missing for electrons) is necessary to assess the possible systematic uncertainties associated with this difference.

Monte Carlo study of the Ne_{+}/Ne_{-} ratio vs scattering electron (positron) angle without included magnetic field was performed for two cases. In the first case both electron (positron) and proton were registered by the TOF detector only (in coincidence). The second case, which corresponds to the real experimental measurements with reconstructed particle tracks, in addition to previous conditions there is also included requirement of registration each particle by the left or right sets of the drift chambers (WC) (which). For each case the 16 million events were generated in the region wider than the detector acceptance region. The magnetic field was not used just to demonstrate the pure effect of annihilation. The results of the simulations (ratios Ne+/Ne-) are presented on the Figs. 1 and 2. Both ratios were fitted with the constant and results of the fitting are presented on the plots.

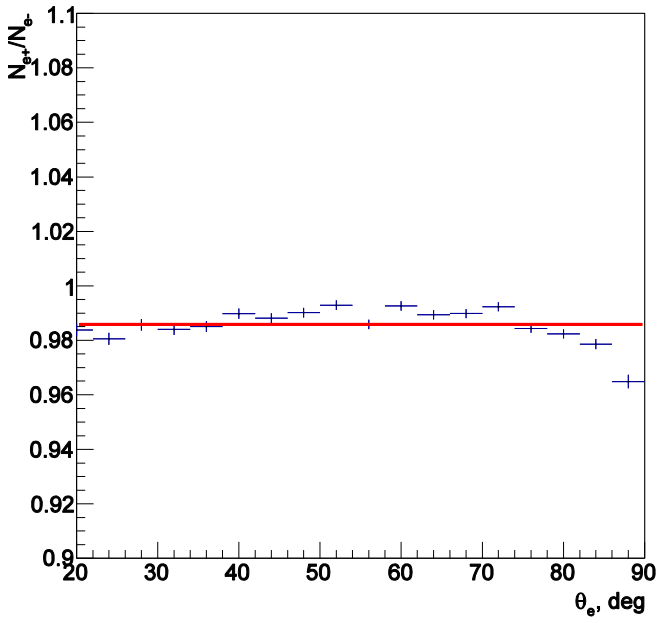

Figs. 1. N_{e+}/N_{e-} ration for the case when electron (positron) and proton from the elastic scattering are both registered just by ToF detector. The result of the fit with constant is: p0= 0.9860 ± 0.0004.

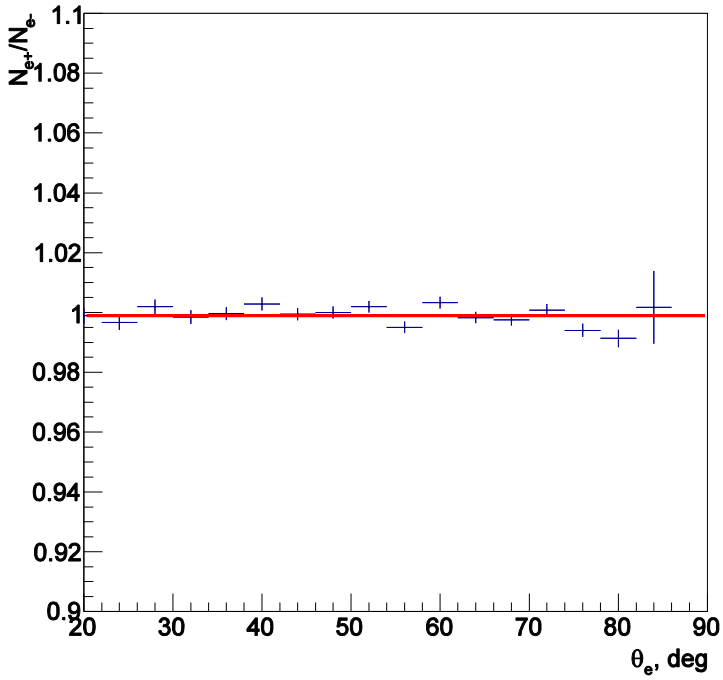

Figs. 2. N_{e+}/N_{e-} ration for the case when electron (positron) and proton from the elastic scattering are both registered by ToF detector and hit three drift chambers (WC). The result of the fit with constant is: p0=0.9991 ± 0.0005

6. Conclusion

As it is follows from the study, the ratio Ne+/Ne- is not uniform for the case when only TOF detector used for the registration. This effect is caused by the annihilation of e+ in e/g/ magnet coils, where there are a lot of materials on the particle path. In the case of using WC in addition to TOF, which corresponds to the real experimental condition (with really reconstructed particles) the ratio of Ne+/Ne- is compatible with 1, the effect of annihilation is not seen which means that the systematics due to this effect is not noticeable.

7. References

- The OLYMPUS collaboration “Technical design report for the OLYMPUS experiment”, july 7, 2010
- А.И.Абрамов и др. “Основы экспериментальных методов ядерной физики”, Атомиздат 1977
- Megh Raj Niroula “Beyond the born approximation: a precise comparison of e^{+}-p and e^{-}p elastic scattering in the cebaf large acceptance spectrometer” 2010
- M.N.Rosenbluth “Phys. Rev.” **79**, 615 1950
- D.Hasell et al. “Nucl. Instr. and Methods in Physics Research” **A603**, 247 2009
- W.Verkerke, D.Kirkdy “RooFit Users Manual v2.91” 2008
- ROOT “A C++ framework for petabyte data storage, statistical analysis and visualization” Antcheva, M.Balintijn, M.Biskup, R.Brun, N.Buncic (CERN), Ph.Canal (Fermilab), D.Casadei (New York U.), 2009